

A NOVEL SWITCHING TECHNIQUE BY dSPACE CONTROLLER FOR DC-DC LLC CONVERTER FOR ELECTRICAL VEHICLE CHARGING

P VAMSI KRISHNA¹, SHAIK SHABANA², KASIBHATLA RAMA SUDHA³, A.CHANDRA SEKHAR⁴

¹Research Scholar, AU College of Engineering, Andhra University, Visakhapatnam, India

² Student, AU College of Engineering, Andhra University, Visakhapatnam, India

³Professor, Department of Electrical Engineering, Andhra University College of Engineering, Visakhapatnam, India.

⁴Professor, Department of Engineering Mathematics, GITAM University, Visakhapatnam, India

ABSTRACT

As the LLC resonant converter excels in efficiency, power density, and input/output voltage control, it is widely used in battery charging applications. High efficiency and power density are becoming more necessary as the market for ultra-fast battery chargers for electric vehicles expands rapidly. LLC resonant converters are popular because of their great efficiency and minimal switching loss. In this research, the small-signal model of a limited-loop-feedback (LLC) resonant converter is developed using the notion of extended description functions. The large-signal limited liability company model is derived using the first-order harmonic approximation technique. These converters are often used in battery chargers, electric cars, and high-efficiency power supply because of the stringent output voltage requirements required by these devices. This paper presents dual-loop control technique, where an inner current loop and an outside voltage loop are established. An LLC dual first order small-signal model with reduced parameters is provided for use in controller design and tuning. For the sake of this study, we will focus on one-loop control (voltage control loop control with LLC). The DC-DC LLC converter with a switching-frequency feed forward. In this paper the main focus was on switching of LLC resonant converter with the help of dSPACE controller which was different from other LLC resonant controllers so that by varying the switching frequency the inductor and capacitor values can be varying in nature for same output voltage so we can practically able to get inductor and capacitor components available for prototype construction. Using mat-lab and Simulink, we propose the gain/phase and pole position at different operational points.

Keywords: *Resonant Converters, Resonant Frequency, Electric Vehicles, State Space Model*

1. INTRODUCTION

More efficient and powerful dc-dc power converters are needed for renewable energy applications [1, 11–13]. Recent years have seen significant advancements in battery technology for use in electric vehicles (EVs). Literature survey has been conducted on how they are using resonant converters. A new approach in current mode control for improving efficiency and to reduce switching losses were given in (jian li et al 2010). Simplified series resonant converter model where this model can predict the dynamic behaviour of circuit and impedance control has been used in (shuilin Tian et al 2016). To further reduction of switching losses and to improve efficiency a small

signal model analysis was given in (chien-hsuan chang et al 2012). An equivalent circuit model for LLC resonant circuit was given for simple small signal analysis and analytical expression for control was given in (shuilin Tian et al 2020). Understanding of resonant converters by describing function analysis for better control model analysis was given in (martin p. Foster et al 2008). Approximation analysis of LLC resonant converters by capacitor filter operation and adding ac resistance for continuous and discontinuous modes were given in (Gregory Ivensky et al 2011). Till date there was no data of controlling of LLC resonant converters by dSPACE, here dSPACE was a controller when we can use it in softare in the

loop or software and hardware in the loop and hardware and hardware in the loop. In this paper LLC resonant converter was built with the help of MATLAB software and the practical results has been shown in results section below.

There are two basic approaches to charging an EV: charging when the vehicle is parked and charging while the vehicle is moving. An on-board charger (OBC) is a device installed in a vehicle that is responsible for controlling the transfer of energy from the power grid into the battery. In order to provide the necessary voltage and current to the car's battery, off-board chargers must coordinate with the vehicle, but their size and weight are less of an issue, thus they may be built for rapid charging. A LLC converter is a common piece of electrical equipment used to convert between two different formats. In addition to the standard series version, a parallel variant of the LLC converter [2] is also on the market. This is the entire bridge converter from an LLC that has isolation built in. Isolated from the noise of the circuit is the full-bridge rectifier and LLC converter. MOSFETS are used in complete bridge rectifier bridges. This circuit uses a diode inverter, a filter, and a resistive load on the output side.

Figure 1 shows a diagram of an LLC converter

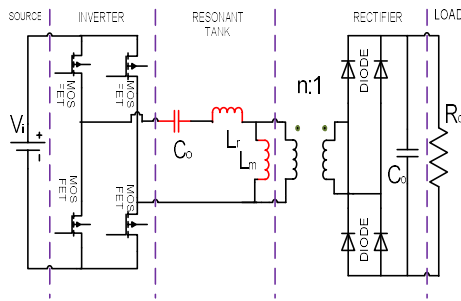


Figure 1 : LLC Converter

1.1 Electrical vehicle

An motor that is powered by electricity rather than a gasoline engine [3]. In-situ charging and charging from a distant location are the two main approaches of charge batteries. Because of the higher level of conduction, recharging a vehicle at a charging station, where it is directly connected to the power grid, is much quicker than charging it at home. When it comes to charging off board, customers have the option of using either their own houses or public charging stations, such as those found in supermarkets. While using an external power

source, it is necessary to devote a significant period of time in order to ensure that the battery of an electric vehicle is completely charged. The AC power is sent directly into the AC/DC converters [4] and the DC supply that is generated by those converters is then connected with DC/DC converters via the use of the DC link. Via the use of DC/DC converters, the battery system, the diode circuit, and the filter were all connected to one another.

1.2 LLC Resonant Converter

The full-bridge rectifier circuit is employed with the LLC converter in this work. Two inductors (Henry) and a capacitor make up the LLC converter, making it one of the reactive element converters (F). The main side of the isolation transformer is linked to a magnetized inductor and the secondary side is connected to the resonant inductor (La) and resonance capacitor (Ca). It is clear from figure 1 that a diode circuit, battery system, and filter are all connected in series on the secondary side of the isolation transformer.

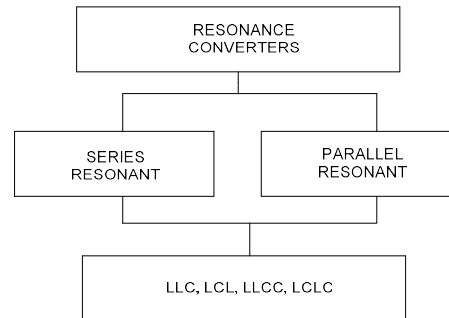


Figure 2 Types of LLC

Power flowing through the converter is controlled by the input frequency in relation to the resonant tank circuit. Semiconductor switching involves gentle switching, zero voltage switching, and zero current switching at both turn-on and turn-off, resulting in a low amount of electromagnetic emission. The great efficiency and power density offered by LLC converters are only two further benefits.

2.0 Mathematical Analysis

The LLC having 4 state variables the resonant inductor current, resonant capacitor voltage, magnetize current, output voltage. They are divided into seven state variables because of first order harmonic.

$$I_{rs} = -w_{sw} i_{rc} + \frac{1}{L_r} \left(\frac{4}{\pi} v_i - v_{cs} - \frac{4}{\pi} n v_o \frac{i_{rs} - i_{rc}}{i_p} \right) \quad (1)$$

$$I_{rc} = w_{sw} i_r - \frac{1}{L_r} \left(V_{cc} - \frac{4}{\pi} n v_o \frac{i_{rc} - i_{mc}}{i_p} \right) \quad (2)$$

$$V_{cs} = -w_{sw} V_{cc} + \frac{1}{C_r i_{rs}} \quad (3)$$

$$V_{cc} = w_{sw} V_{cs} + \frac{1}{C_r i_{rc}} \quad (4)$$

$$I_{ms} = -w_{sw} i_{mc} + \frac{1}{L_m} \left(\frac{4}{\pi} n v_o \frac{i_{rs} - i_{rc}}{i_p} \right) \quad (5)$$

$$I_{mc} = w_{sw} i_{ms} + \frac{1}{L_m} \left(\frac{4}{\pi} n v_o \frac{i_{rc} - i_{mc}}{i_p} \right) \quad (6)$$

$$\dot{v}_o = \frac{1}{C_o} \left(\frac{2}{\pi} n i_p - \frac{v_o - v_b}{R_b} \right) \quad (7)$$

$$S = \begin{bmatrix} 0 & 0 & 0 & 0 & 0 & 0 & 0 \\ 0 & 0 & 0 & 0 & 0 & 0 & 0 \\ 0 & 0 & 0 & 0 & 0 & 0 & 0 \\ 0 & 0 & 0 & 0 & 0 & 0 & 0 \\ 0 & 0 & 0 & 0 & 0 & 0 & 0 \\ 0 & 0 & 0 & 0 & 0 & 0 & 0 \\ 0 & 0 & 0 & 0 & 0 & 0 & 1 \end{bmatrix} \quad (9)$$

$$R = \begin{bmatrix} -26.98 \\ 58.92 \\ -62.55 \\ -28.64 \\ -27.55 \\ 27.05 \\ 0 \end{bmatrix} \quad U = \begin{bmatrix} 0 \\ 0 \\ 0 \\ 0 \\ 0 \\ 0 \\ 0 \end{bmatrix} \quad (10)$$

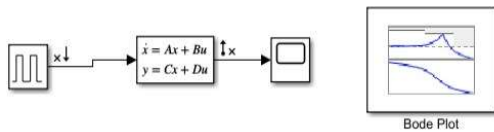


Figure 3 Simulation Model

The seven values in the state space, represented by the equations 1–7, are the sine and cosine derivatives. Analysis of the state space of a seventh-order LLC system is provided in Equations 8 and 9. As shown in Fig.3, the 7th order LLC state space analysis makes use of the pulse generator as an input block, a linear state space block, and an output scope. Enter the state space matrix (P, R, S and U) into the linear state space block. The input block is treated as open loop input, and the output is treated as open loop output, making this a circuit with an open loop. The output is shown as a gain and phase, and a bode plot block is dumped from Matlab's library so that the user may see the data. Run the whole block diagram along the bode by opening the plot using the bode's information, dumping your data there by clicking an arrow, and then setting the open-loop input to input perturbation and the open-loop output to output measurement. The following is a state space analysis of a seventh-order system, where P is the state space variable, R is the input vector, S is the output vector, and U is the feedback vector.

$$AX+BU, CX+DU$$

$$P = \begin{bmatrix} -0.015e4 & -64.3e4 & -60.6e4 & 0e4 & 0.015e4 & 1.54e4 & -38.6e4 \\ 61.3e4 & -157e4 & 0e4 & -60.6e4 & 1.54e4 & 157.4e4 & 0.38e4 \\ 66.7e4 & 0e4 & 0e4 & -62.8e4 & 0e4 & 0e4 & 0e4 \\ 0e4 & 66.7e4 & 62.8e4 & 0e4 & 0e4 & 0e4 & 0e4 \\ 0.0028e4 & 0.29e4 & 0e4 & 0e4 & -0.0028e4 & -63.1e4 & 7.2e4 \\ 0.29e4 & 29.5e4 & 0e4 & 0e4 & 62.5e4 & -29.5e4 & -0.07e4 \\ 0.009e4 & -0.00009e4 & 0e4 & 0e4 & -0.009e4 & 0.00009e4 & -0.002e4 \end{bmatrix} \quad (8)$$

In order to employ the Jacobian matrix at the appropriate switching frequency, the values of the state matrix are determined by averaging the results of the small permutation approach. Using the order reduction technique, the 7th order system was simplified to the 1st order. The dominant poles are shown on the left side of the root-locus when applied to a system of seventh order. The order of the system decreases when the poles and zeros that are far from the zero axis are eliminated (the order of the system depend on the poles and zeros). The order of the systems discussed in this article ranges from the seventh to the first. L (1st order), R (1st order), V (1st order), etc., are all first-order components that are equal to one another.

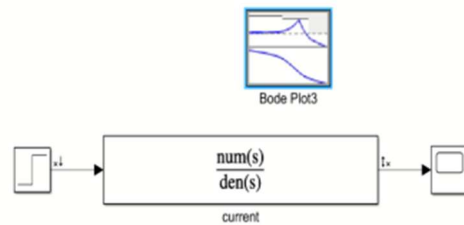


Figure 4 Simulation Model

$$L_{Equi} = \frac{\pi^2}{8n^2} L_{resonant} \left(1 + \frac{F_{sw}^2}{f_{ressonant}^2} \right) \quad (11)$$

$$R_{Equi} = \frac{\pi^2}{8n^2} R_{load} \quad (12)$$

$$V_o = 2\pi G_{pade} F_{sw} \quad (13)$$

$$V_{1storder} = \frac{\pi}{2n} \left(2\pi K_e F_{sw} + 2\pi G_{pade} F_{sw} * R_{load} \right) \quad (14)$$

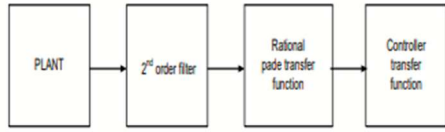


Figure 5 Simulation Model.

Equations 10-14 are the first-order ones for plants. Fig.5 shows a block diagram of an open-loop voltage controller, which consists of the plant, the second-order filter, the rational-pade transfer function, and the controller transfer function. Since it is a digital operation, the second-order filter may be run at a constant sampling time and utilized to smooth out voltage and rational-pade transfer-function fluctuations (Ts). To maintain a steady state, the controller transfer function controls the switching frequency such that it is lower than the resonant frequency. Equation 15 describes the transfer function of a second-order filter when it is applied to a current measurement. Equation 16 describes the transfer function of a Pade filter, while

$$G_{2^{nd} \text{ order}(i)}(s) = \frac{w_{2^{nd} \text{ order filter}}^2}{(s + w_{2^{nd} \text{ order filter}})^2} \quad (15)$$

$$G_{\text{pade}(i)}(s) = \frac{1 - s \frac{T_s}{4}}{1 + s \frac{T_s}{4}} \quad (16)$$

$$G_{\text{plant}(t.f)}(s) = \frac{i_{\text{output}}}{F_{sw}} \approx \frac{h_{\text{ssg}(i)}}{1 + \frac{s}{w_{\text{pole}(i)}}} \quad (17)$$

$$h_{\text{ssg}(i)} = g * h \quad (18)$$

Where

$$g = \frac{1}{F_{sw}}$$

$$h = \frac{\frac{\pi}{2n}(2\pi K_e F_{sw} + 2\pi G_{\text{pade}} F_{sw} * R_{\text{load}})}{\frac{\pi^2}{8n^2} R_{\text{load}}}$$

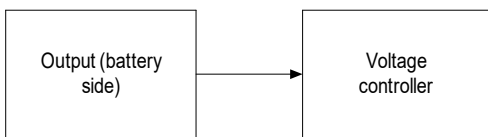


Figure 6 Simulation Model

Fig.6 shows the block diagram of the voltage controller on the battery side, which is in charge of controlling the output current and hence the voltage across the filter capacitor. The voltage regulator's output is being filtered to remove any Equations 17

and 18 describe the transfer function of a plant. Maintaining a 19-year upward trend. A frequency of 20 Hz at the pole. Function of the controller at the output in equation (21); frequency of the open loop cross over in equation (22); transfer function of the current regulator at the output in equations (23) and (24); function of the battery at the output in equation (25); function of the controller at the output in equation (26); and function of the regulator at the output in equation (27)

$$W_{\text{pole}(f)(i)} = \frac{\frac{\pi^2}{8n^2} R_{\text{load}}}{\frac{\pi^2}{8n^2} L_{\text{resonant}} (1 + \frac{F_{sw}^2}{f_{\text{resonant}}^2})} \quad (19)$$

$$G_{\text{controller}(t.f)(i)} = i * j \quad (20)$$

Where

$$i = \frac{1}{h_{\text{ssg}(i)}}, j = \left(\frac{1}{w_{\text{pole}(f)(i)}} w_{\text{crossover}(i)} + \frac{w_{\text{crossover}(i)}}{s} \right)$$

$$w_{\text{crossover}(i)} = k_{\text{proportional}(i)} = k_{\text{integral}(i)} \quad (21)$$

$$G_{\text{open loop}(t.f)(i)} = a * b \quad (22)$$

where

$$a = \left(G_{2^{nd} \text{ order}(i)}(s) \right) \left(G_{\text{pade}(i)}(s) \right)$$

$$b = \left(G_{\text{controller}(t.f)(i)} \right) \left(G_{\text{plant}(t.f)}(s) \right)$$

$$G_{\text{open loop}(t.f)(i)} = c * d \quad (23)$$

where

$$c = \left(G_{2^{nd} \text{ order}(i)}(s) \right) \left(G_{\text{pade}(i)}(s) \right)$$

$$d = \left(G_{\text{controller}(t.f)(i)} \right) \left(\frac{\frac{1}{F_{sw}} \frac{V_{\text{Equi}}}{R_{\text{Equi}}}}{1 + s \frac{L_{\text{Equi}}}{R_{\text{Equi}}}} \right)$$

$$G_{\text{battery plant}}(s) = \left(\frac{R_{\text{battery}}}{1 + s R_{\text{battery}} C_{\text{out}}} \right) \quad (24)$$

$$G_{\text{control}(t.f)(v)}(s) = k_{\text{proportional}(v)} + \frac{k_{\text{integral}(v)}}{s} \quad (25)$$

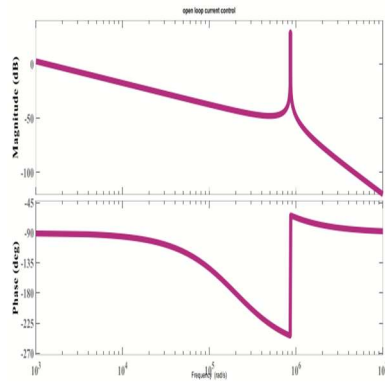


Figure 7 Plant Transfer Function Bode

unwanted disruptions. The battery management system (BMS) ensures that the battery is always being charged from the source of power.

$$G_{\text{open loop}}(s) = e * f \tag{26}$$

where

$$e = \left(\frac{R_{\text{battery}}}{1 + sR_{\text{battery}}C_{\text{out}}} \right)$$

$$f = \left(G_{\text{control(t.f)(v)}(s)} \right)$$

$$k_{\text{proportional(v)}} = w_{\text{cross over(v)}} * C_{\text{out}} \tag{27}$$

3. RESULTS

Fig. 7 shows a bode plot for the plant's transfer function, whereas Fig. 8 displays a bode plot for open-loop control. Open loop voltage control is seen in Fig. 9 The open loop bode plot is shown in Fig.10. The open loop transfer function is the sum of the pade transfer function, the zero order hold transfer function, and the pi controller, the values of which are shown in Fig. 7. The open loop cross over frequency at 0 dB is used as the proportional gain value in the Pi Controller. The desired phase margin is a measure of the frequency at which the two signals cross. The phase margin is set at 50 degrees here (degree). The 25 kHz second order filter. The phase and magnitude plot of the open loop of the voltage controller is shown in fig.8 below. The inner loop control is a voltage regulator's alternative name. As it stands, the frequency at which the open loop cross over occurs at 0 dB is much below the frequency at which the cross over occurs at the moment. Assume a frequency of 110 kHz for the open loop cross over. A feedback connection from the pi controller is

made to the resonant converter. The voltage control's cross-over frequency of 5 helps boost the closed-loop system's ability to dampen disturbances.

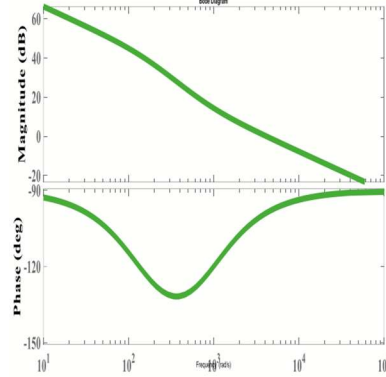


Figure 8 Plot For Magnitude Vs Frequency And Phase Vs Frequency Of Open Loop Voltage Control

with the use of the voltage gain and quality factor with regard to the switching frequency, the resonant frequency can be determined to be 140 kHz and the switching frequency to be 109 kHz (fig.9), with the resonant impedance being 7.7 ohms. There is a 405 volt difference between the input and output voltages of 325 volts. When the switching frequency is higher than the resonant frequency, as shown in fig.10, the transfer function of the plant changes. The output voltage is 215 volts. Voltage gain is 0.66, and the input voltage is 325 volts.

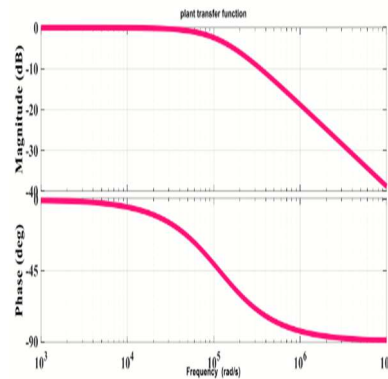


Figure 9 Plot For Magnitude Vs Frequency And Phase Vs Frequency.

The seven state variables with regard to the switching frequency are shown in a phase and magnitude plot of the seventh order state space analysis matrix in fig.11. All derivatives have zero as their value.

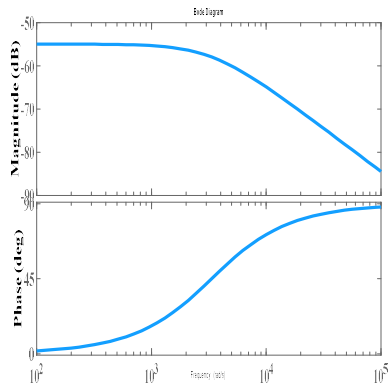


Figure 10 Plot For Magnitude Vs Frequency And Phase Vs Frequency

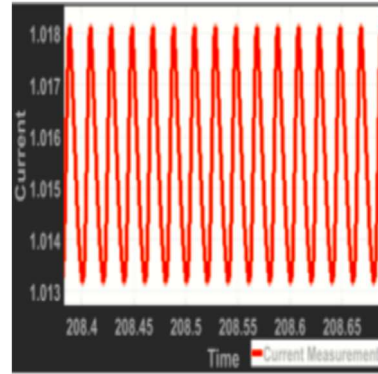


Figure 12 Output Voltage In Boost Mode

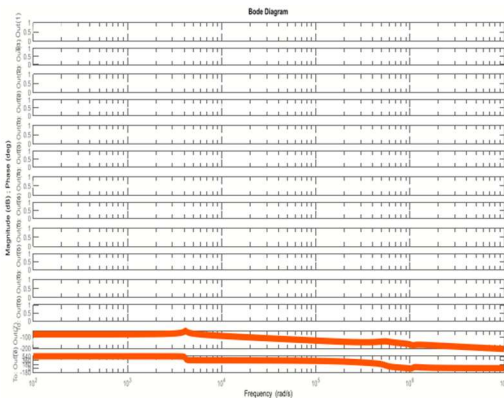


Figure 11 Simulation Result Plot For Magnitude Vs Frequency And Phase Vs Frequency Of State Space Analysis Of 7th Order System.

3.1 Resonant converter results

Using matlab and simulink, we were able to determine that the output voltage of an LLC converter without a pid controller is 8.81 volts, and that the output current magnitude is 1 ampere. The input voltage is 8 volts, and the switching frequency is 50 hertz; because the switching frequency is less than the resonant frequency, the LLC converter operates in boost mode.

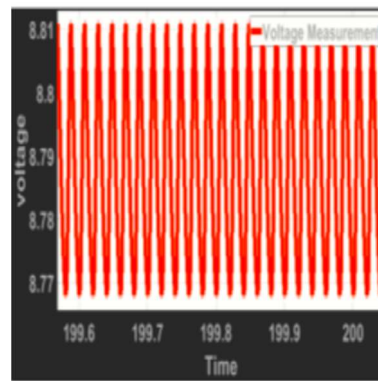
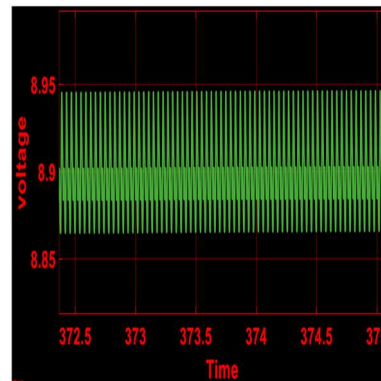


Figure 13 Output Current

3.2 Resonant converter with pid controller: The results of a PID-controlled LLC converter are shown in Fig. 14. By adjusting the PID controller's proportional and intergral gains, we were able to increase the output voltage of the LLC converter operating in boost mode to 8.95 volts, very close to the theoretical maximum of 9 volts. When the switching frequency is smaller than the resonant frequency, the current value exceeds 1A, which is higher than it is for the LLC converter with pid and the LLC converter without pid controller.



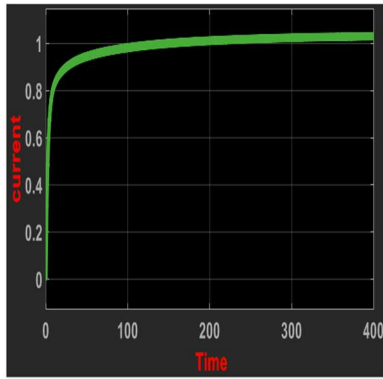


Figure 14 The LLC Outputs With PID Controller

3.3 Stability analysis

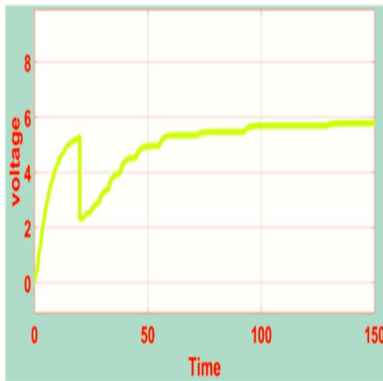


Figure 15 Plot with disturbance.

Stability study of the LLC converter is shown in fig.15 above; it was obtained by coupling the pid controller to the LLC resonant converter and subjecting it to minor disturbances for 20 seconds. An application of 4.5 volts causes the disturbance 20 seconds later. The signal stabilizes between 70 and 150 seconds after 20 seconds, with a magnitude of 5 Volts.

3.4 Dspace analysis

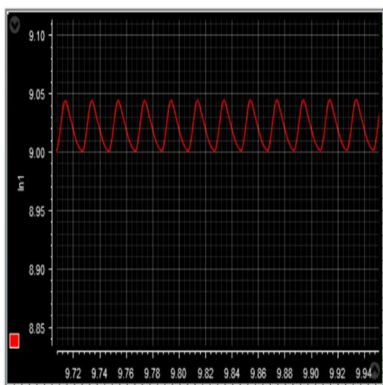
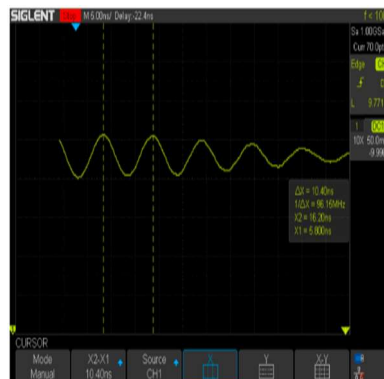


Figure 16 dSPACE output voltage waveform

With the help of the Dspace to matlab interface, we were able to increase the output voltage of the LLC resonant converter by a factor of 9 volts; in this case, the LLC converter has a voltage gain of 1 and the resonant inductance and capacitor values are 13.78H and 736.89 micro F, respectively, as shown in Fig.16.

3.5. Proto type results: The boost mode outputs of an LLC converter prototype are shown in fig.16 below. Figures 14 and 13 as well as Figure 15 represent the practical type outputs of an LLC converter operating in boost mode, as determined by the study of practical types. In a steady state operation, the output voltage may approach 9V and the current can approach 1A. With the same inductor and capacitor settings as the prototype, the LLC's quality factor, output voltage, and current values all approach 10V and 1A, respectively. The output voltage is 10 volts, as shown in the first figure of the prototype findings.



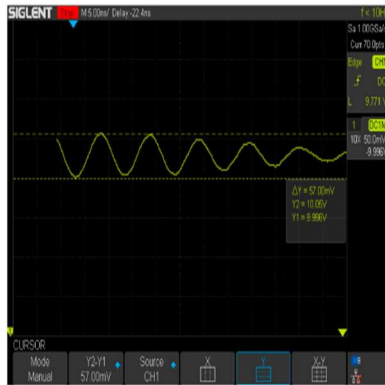


Figure17 Prototype LLC Converter Output Voltage Waveforms

Table 1 Parameters Of The Prototype Model

Resonant inductor Lr	14 milli H
Resonant Capacitor Cr	736.0 Micro F
Quality Factor	0.5
Voltage gain, M	1
Magnetizing current, Lm	68 Milli H
Equivalent resistance	9 ohm

4. COMPARATIVE ANALYSIS

In the literature review all the work was focusing on small signal analysis and to reduce switching losses by various techniques, in this paper the controlling of the switches was with the help of dSPACE controller. Coming to pros, here we can change the switching frequency so that inductor and capacitor values can be variable in nature so the size and weight of the circuit can be reduced. Coming to cons, in this the dSPACE controller has some practical limitations for hardware and software in the loop where the switching frequency was limited to 10 kHz.

5. CONCLUSION

Analysis of the LLC converter for charging electric vehicles is performed using the small signal model and the average model of the seventh order system. Two useful modes for controlling voltage and current are the output side voltage control mode and the inner current control mode. Bode graphs illustrate the enhanced adaptive gain of the battery pack for electric vehicles. Inductance, capacitance, transformer ratio, input and output voltages are all computed and shown in Figure 1 for a resonant

converter with a resonance frequency of 50 Hz. All of this is simulated in Matlab, and the results are shown up there. It is on the basis of these numbers that the prototype is built, and it is the waveforms at the output that are shown above. The contributions in this work are software in the loop installation with the help of dSPACE controller the practical outputs are taken and shown in results section in addition to this stability analysis was also done. The future scope of this work is implementation of charging stations with the help of LLC resonant converters for these charging stations installation economic estimations can be done with the help of system advisory model (SAM) software and can be implemented for village communities.

REFERENCES:

- [1] Davide Cittanti, Matteo Gregorio, Enrico Vico, Fabio Mandrile, Eric Armando, Radu Bojoi. "High Performance Digital Multi-Loop Control of LLC Resonant Converters for EV Fast Charging with LUT-Based Feedforward and Adaptive Gain", IEEE Transactions on Industry Applications, 2022.
- [2] Franco Degioanni, Ignacio Galiano Zurbriggen, Martin Ordonez. "Dual-Loop Controller for Resonant Converters Using an Average Equivalent Model ", IEEE Transactions on Power Electronics, 2018.
- [3] Davide Cittanti, Matteo Gregorio, Eric Armando, Radu Bojoi. "Digital Multi-Loop Control of an LLC Resonant Converter for Electric Vehicle DC Fast Charging", 2020 IEEE Energy Conversion Congress and Exposition (ECCE), 2020
- [4] Yixian Ma, Yun Wei, Hua Yang, Xin Cheng, Chen Zhang, Xuehua Wang. "Small-Signal Modeling of LLC Resonant Converters", 2020 IEEE International Conference on Information Technology, Big Data and Artificial Intelligence (ICIBA), 2020.
- [5] GL Arnold, C Bertrand, F Feillet, T Hashimoto et al. "Development of a Tandem Mass Spectrometry Method for Rapid Measurement of Medium- and Very-Long-Chain Acyl-CoA Dehydrogenase Activity in Fibroblasts", Springer Science and Business Media LLC'
- [6].M.S. Kim, S.B. Dewan. "Closed-loop voltage regulation of dual converters with circulating-current mode, used in four-

- quadrant DC magnet power supplies", IEEE Transactions on Industry Applications, 1991
- [7] Yuqi Wei, Quanming Luo, Si Chen, Pengju Sun, Necmi Altin. "Comparison among different analysis methodologies for LLC resonant converter", IET Power Electronics, 2019.
- [8] Duerbaum, "First Harmonic Approximation Including Design Constraints," in International Telecommunications Energy Conference (INTELEC), San Francisco, CA, USA, 1999, pp. 321–328.
- [9] S. De Simone, C. Adragna, C. Spini, and G. Gattavari, "Design-Oriented Steady-State Analysis of LLC Resonant Converters Based on FHA," in International Symposium on Power Electronics, Electrical Drives, Automation and Motion (SPEEDAM), Taormina, Italy, 2006, pp. 200–207.
- [10] C.-H. Chang, E.-C. Chang, C.-A. Cheng, H.-L. Cheng, and S.-C. Lin, "Small Signal Modeling of LLC Resonant Converters Based on Extended Describing Function," in International Symposium on Computer, Consumer and Control (IS3C), Jun. 2012, pp. 365–368.
- [11] C. Buccella, C. Cecati, and H. Latafat, "Digital Control of Power Converters — A Survey," IEEE Transactions on Industrial Informatics, vol. 8, no. 3, pp. 437-447, Aug. 2012.
- [12] H.-P. Park and J.-H. Jung, "PWM and PFM Hybrid Control Method for LLC Resonant Converters in High Switching Frequency Operation," IEEE Transactions on Industrial Electronics, vol. 64, no. 1, pp. 253–263, Jan. 2017. [13] Z. Fang, T. Cai, S. Duan, and C. Chen, "Optimal Design Methodology for LLC Resonant Converter in Battery Charging Applications Based on Time-Weighted Average Efficiency," IEEE Transactions on Power Electronics, vol. 30, no. 10, pp. 5469–5483, Oct. 2015.
- [14] S. Tian, "Equivalent Circuit Model of High Frequency Pulse- Width Modulation (PWM) and Resonant Converters," Ph.D. dissertation, Virginia Tech, Aug. 2015.
- [15] T. Nussbaumer, M. L. Heldwein, G. Gong, S. D. Round, and J. W. Kolar, "Comparison of Prediction Techniques to Compensate Time Delays Caused by Digital Control of a Three-Phase Buck-Type PWM Rectifier System," IEEE Transactions on Industrial Electronics, vol. 55, no. 2, pp. 791–799, Feb. 2008.
- [16] D. Cittanti, M. Gregorio, F. Mandrile, and R. Bojoi, "Full Digital Control of an All-Si On-Board Charger Operating in Discontinuous Conduction Mode," Electronics, vol. 10, no. 2, p. 203, Jan. 2021.